Lab on a Chip

Accepted Manuscript

This is an *Accepted Manuscript*, which has been through the RSC Publishing peer review process and has been accepted for publication.

Accepted Manuscripts are published online shortly after acceptance, which is prior to technical editing, formatting and proof reading. This free service from RSC Publishing allows authors to make their results available to the community, in citable form, before publication of the edited article. This *Accepted Manuscript* will be replaced by the edited and formatted *Advance Article* as soon as this is available.

To cite this manuscript please use its permanent Digital Object Identifier (DOI®), which is identical for all formats of publication.

More information about *Accepted Manuscripts* can be found in the **Information for Authors**.

Please note that technical editing may introduce minor changes to the text and/or graphics contained in the manuscript submitted by the author(s) which may alter content, and that the standard **Terms & Conditions** and the **ethical guidelines** that apply to the journal are still applicable. In no event shall the RSC be held responsible for any errors or omissions in these *Accepted Manuscript* manuscripts or any consequences arising from the use of any information contained in them.

RSC Publishing

www.rsc.org/loc
Registered Charity Number 207890

A passive droplet sorting scheme based on intrinsic viscoelastic fluid properties to efficiently sort droplets in a high throughput fashion.

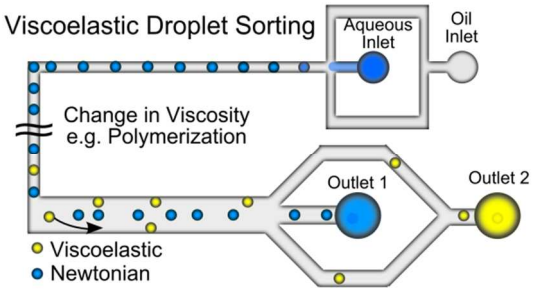

View Article Online

Cite this: DOI: 10.1039/c0xx00000x

www.rsc.org/xxxxxx

ARTICLE TYPE

Passive Droplet Sorting using Viscoelastic Flow Focusing

Andrew C. Hatch,[a] Apurva Patel,[a] N. Reginal Beer,[b] and Abraham P. Lee*[a]

Received (in XXX, XXX) Xth XXXXXXXXX 20XX, Accepted Xth XXXXXXXXX 20XX
DOI: 10.1039/b000000x

We present a study of passive hydrodynamic droplet sorting in microfluidic channels based on intrinsic viscoelastic fluid properties. Sorting is achieved by tuning the droplets' intrinsic viscous and viscoelastic properties relative to the continuous oil phase to achieve a positive or negative lateral migration toward high or low shear gradients in the channel. In the presence of weakly viscoelastic fluid behavior, droplets with a viscosity ratio, κ, between 0.5-10 were found to migrate toward a high shear gradient near the channel walls. For all other κ -values, or Newtonian fluids, droplets would migrate toward a low shear gradient at the channel centerline. It was also found that for strongly viscoelastic fluids with low interfacial tension, droplets would migrate toward the edge even with κ-values lower than 0.5. The resulting bi-directional lateral droplet migration between different droplets allows size-independent sorting. Still, their sorting efficiencies are dependent on droplet size, intrinsic fluid elasticity, viscosity, droplet deformability, and overall fluid shear rates. Based on these findings, we demonstrate >200 Hz passive droplet sorting frequencies and achieve >100 fold enrichment factors without the need to actively sense and/or control active mechanisms. Using a low viscosity oil phase of 6.25 cPs, we demonstrate sorting discrimination of 1 cPs and 5 cPs aqueous droplets with κ-values of 0.2 and 0.8 respectively.

Introduction

On chip droplet detection and sorting based on different contents is useful for microfluidic based quantitative analysis, product enrichment, and sample isolation during both pre- and post-processing[1–5]. One limiting factor of active droplet sorting techniques is the sensing and sorting mechanisms they require. This then complicates fabrication, use, cost, energy demands of the device, and complicates massively parallel designs[1,6–8]. Common droplet properties that may vary from drop to drop include size, density, interfacial tension, viscosity, stiffness, optical, electrical, magnetic, acoustic, or thermal properties. Size based droplet sorting using hydrodynamic flow focusing has proven useful because it reliably differentiates between droplets based on unique size variations[3–5,9,10]. However, droplet microfluidic chips are often used to produce and manipulate monodisperse droplet sizes[11,12], making size based sorting insufficient for many applications where passive separation is desired. The ability to passively sort droplets based on more than one intrinsic property is useful for chemical and biological applications that require enrichment of specific intrinsic material properties. In this work, we explore experimental research in the context of viscous and viscoelastic based droplet migration in microfluidic channels for passive, on-chip droplet separation.

Motion of rigid particles[13–15] and droplets[16–19] in laminar flow viscous fluids has long been investigated and characterized in theoretical fluid mechanics studies. Of particular interest, work by Chan and Leal (1979) describe that in second order fluids with a unidirectional flow, cross-stream/lateral migration of deformable droplets occurs toward the walls when viscosity ratios, κ, of the inner and outer fluid phase is between 0.5-10, and inversely, toward the center for all other κ-values[16]. Several recent works further investigate particle focusing, and droplet migration in various channel geometries and flow regimes including viscoelastic, inertial, and Deans flow conditions[20–31]. In particular, it is understood that rectangular channels have several local minima and maxima shear gradient positions making hydrodynamic flow focusing of particles, bubbles, and droplets in square and rectangular channels more complex compared to circular channels[30–34]. Figure 1 illustrates some of the various droplet migration forces that might influence the cross-lateral migration of a deformable droplet in square or rectangular channels under laminar flow conditions.

In this work we investigated the empirical behavior of Newtonian and Non-Newtonian water in oil droplets in straight and curved rectangular channels to determine effectual sorting parameters based on changes in droplet viscosity. Other design parameters we discuss include the influence of channel geometry, droplet size, droplet starting position, and fluid flow rates on droplet equilibrium positions for high-throughput droplet sorting. We further demonstrate that an inversion in droplet migration direction provides a useful droplet separation scheme to yield a positive or negative bi-modal sorting parameter by tuning the viscoelasticity and viscosity ratio of the fluid phases in or out of the $0.5 < \kappa < 10$ regime. This explicit dependence on κ to determine migration direction decreases sorting dependence on droplet size, interfacial tension, or shear rate. Passive on-chip droplet sorting of aqueous droplets is achieved by relying on

View Article Online

Cite this: DOI: 10.1039/c0xx00000x

www.rsc.org/xxxxxx

ARTICLE TYPE

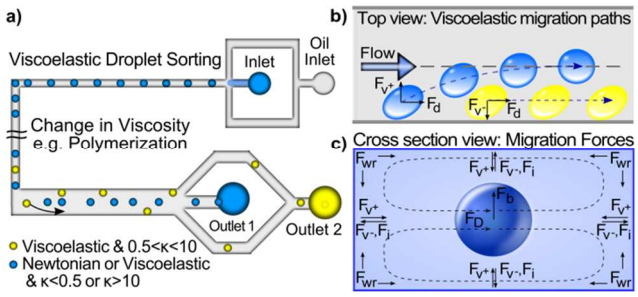

Fig. 1 Illustration of viscoelastic droplet sorting based on bi-modal equilibrium positions. **a)** Viscoelastic droplets with κ -values between 0.5-10 (yellow) migrate toward high shear gradients at the edge, (F_{v-}), while all others (blue) migrate toward low shear gradients at the center, (F_{v+}). **b)** Droplet migration forces including drag forces, F_d, and positive and negative viscoelastic forces result in different migration paths. **c)** Cross-sectional view of droplet migration forces acting on a droplet in a rectangular microfluidic channel. Forces include buoyancy, F_b, wall repulsion forces, F_{wr}, positive or negative viscoelastic forces, F_{v+} and F_{v-} respectively, and in the case of high Reynolds number, inertial forces, F_i, which act in the same direction as F_{v-}. For curved channels, recirculating Deans forces, F_D, illustrated with dashed lines, may also occur.

intrinsic changes of Newtonian and non-Newtonian droplet viscosity as illustrated in Figure 1. This approach enables separation of both monodisperse and moderately polydisperse droplet size populations based on viscosity and viscoelasticity differences, yielding bi-modal droplet migration and sorting.

Theory

Based on research by Chan and Leal[16,17] for second order fluids, deformable droplets propagating in a unidirectional Poiseuille or simple shear fluid flow will experience a transverse shear gradient that induces cross-stream droplet migration. The direction and magnitude of the cross-stream migration, μ_m, in Poiseuille flow is described in equation 1 as a function of droplet size, a, interfacial tension, γ, and other fluid flow properties as:

$$\mu_m = 16\alpha\frac{\mu_o}{\gamma}V_m^2\frac{a^3}{d^3}\left(1-2\frac{y}{d}\right) \quad (1)$$

Here d is the distance between two parallel plane walls; y is the droplet position between the droplet center and nearest wall, μ_i and μ_o are the inner and outer fluid phase viscosity respectively. V_m is the maximum fluid velocity which occurs at $y=d/2$ and is approximated as $Vm \approx 3V_{avg}/2$, where V_{avg} = average fluid velocity. The term α depends on the inner to outer fluid phase viscosity ratio, $\kappa = \mu_i / \mu_o$, and is defined for three-dimensional quadratic shearing flow in equation 2 as follows:

$$\alpha = \frac{1}{(1+k)^2(2+3k)}\left[\frac{3}{14}\times\frac{16+19k}{(2+3k)}(1-k-2k^2) + \frac{10+11k}{140}(8-k+3k^2)\right] \quad (2)$$

Their findings described that in the presence of a second-order fluid in one or both fluid phases of an emulsion, a sign inversion of the term α occurs between the viscosity ratio $0.5 < \kappa < 10$ as illustrated in Figure 2 a). The sign inversion in α causes a transverse droplet migration in two different directions, a positive value migrates toward a low shear gradient and a negative value migrates toward a high shear gradient. This work aims to test this theory on viscoelastic fluids for droplet sorting. This would provide a useful droplet separation scheme by tuning the degree of non-Newtonian behavior and viscosity ratio, κ, in or out of this regime to yield a bi-modal, positive or negative, sorting parameter as illustrated in Figure 2 b).

One beneficial advantage of this expected behavior is that although migration rates depend heavily on droplet size, interfacial tension, and overall shear rate, the ultimate equilibrium point of the droplets will be less dependent on these parameters provided there is ample channel length to reach equilibrium conditions. Another observation from equation 2 is that the rate of droplet migration depends on the starting droplet position within the channel, showing greater migration rates closer to the wall. Figure 2 c) illustrates the differences in theoretical droplet migration, and total separation of two droplets, as a function of downstream propagation for different lateral starting positions, y.

Recent works have been performed to further investigate droplet migration characteristics outside the limits imposed by Chan and Leal's simplified fluid flow conditions of second order fluids. In particular the influence of Capillary number, Ca, Reynolds number, Re, droplet to wall separation, s=y/d, droplet diameter to plane wall spacing, ζ = a/d, the ratio of internal and external fluid Weissenberg numbers, δ=Wii/Wio, and channel geometries have all been identified as important parameters[30,32,35]. Their findings illustrate that these factors can have significant contributions to droplet deformation, localized internal shear rates, and cross-lateral migration rates[25,34,36–40]. Additionally, some works have claimed to observe cross-lateral migration contrary to those of Chan and Leal, but further investigation to their experimental conditions suggest that their fluids were strictly Newtonian, or not sufficiently viscoelastic[36,37,34]. This would suggest that there still exists some degree of confusion over the nature of fluid migration of Newtonian and non-linear/viscoelastic fluids.

As best that can be ascertained from the literature, work by Sullivan et al. (2008) is the only experimental work to demonstrate lateral migration of a deformable sphere away from the channel centerline while having a κ-value outside the range of 0.5-10. Their work investigated the influence of interfacial tension and surfactant additives on transverse bubble migration in viscoelastic fluids, an interesting case since air bubbles are compressible fluids of such low viscosity that they are limited to the condition of $\kappa \ll 1$ [41]. They found that migration of a bubble toward the channel wall only occurred in the presence of a highly

View Article Online

Cite this: DOI: 10.1039/c0xx00000x

www.rsc.org/xxxxxx

ARTICLE TYPE

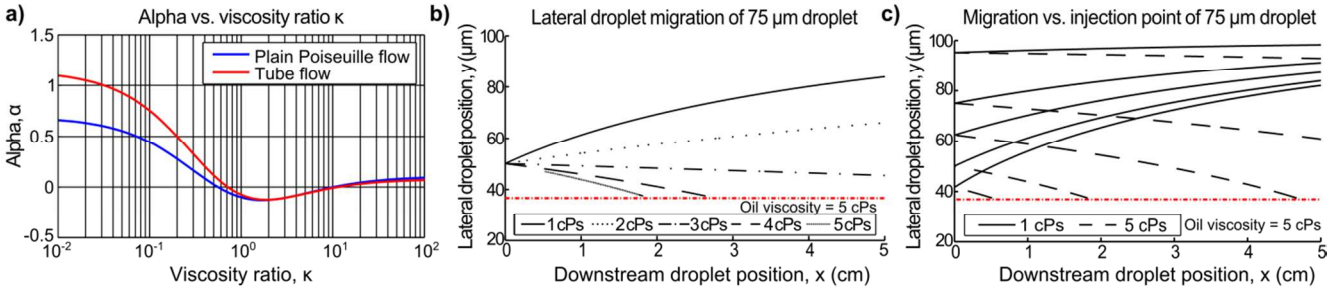

Fig. 2 Theoretical modeling of viscoelastic droplet migration **a)** plot of alpha, α, as a function of viscosity ratio, k. Note that between the range of ~0.5 < κ < 10, α is negative with a global minimum at κ =1. **b)** Projected positive and negative droplet migration of 75 µm droplets of various viscosities. **c)** Migration of droplets with various lateral starting positions, y. Conditions: 20 µl/min flow rate; 100 x 200 µm channel; interfacial tension 15 N/m; Ca=.008, Re=0.8. Red dashed lines in b) & c) indicate 37.5 µm distance where droplets contact the wall and migration nears its limit.

viscoelastic continuous fluid phase with a low interfacial tension as demonstrated through the addition of polyethylene oxide and Tween 20 surfactant. For further discussion pertaining to theoretical background, please refer to ESI section I.

Experimental

Device fabrication

Microfluidic devices were patterned in Polydimethylsiloxane (PDMS) using standard soft lithography processes[42,43] and bonded to glass slides using air plasma treatment to seal the microfluidic channels. Microfluidic master molds of SU-8 2050 (MicroChem) on 3" silicon wafers were fabricated in a class 1,000 clean-room facility and their thickness measured using a Dektak profilometer (Veeco). Sylgard-184 PDMS (Dow Corning) was cast on top of the SU-8 molds then cured in a 60 °C oven for 12-24 hours. The microfluidic devices were assembled by coring inlet and outlet holes in the PDMS layer then bonding them to 1 mm thick borosilicate 1"x3" or 2"x3" glass slides(Corning, USA) using air plasma treatment (Harrick Plasma, USA) at 250 mTorr for 2 min at 200 W power. Finally, the entire device was placed in a 120 °C oven overnight to restore the material to its native hydrophobic condition.

Several different shear sorting channel geometries were tested during these experiments ranging from straight, curved, and gradually widening channels. Channel heights were varied from 40-135 µm and width varied from 50-500 µm as both straight and curved channels varying in length from 0.5 cm to 12 cm. Longer channels with gradually increasing widths were patterned using a spiral configuration ranging from 60-100 µm wide inlets to 400-500 µm wide outlets at different expansion rates and radii of curvature. The primary microfluidic designs used for observing droplet migration are illustrated in ESI Figures S1 & S2. All devices consisted of one or two shear-focusing droplet generators to form the droplet emulsions. The outlets had 1, 3, or 5 bifurcating channels to characterize sorting efficiencies.

Flow rates and shear gradient profiles

ESI Figure S3 illustrates flow rate and shear rate profile simulations in square and rectangular channels under laminar Poiseuille flow ranging from a height/width, h/w, aspect ratio of 1:1 to 1:5. To achieve both a rapid droplet migration rate and a large droplet separation at the outlet, channel widths started out small then gradually increased to yield rapid droplet migration at the beginning of the channel and larger separation from channel edge to center towards the end of the channel. Such channels will have gradually decreasing shear rates and changes in the max and min shear gradient profiles causing droplets to experience continuously varying conditions as they propagate downstream. The average velocity through a channel was determined as $V_{avg}=Q_o/hw$ where Q_o is the total flow rate and h and w are the channel height and width respectively. The non-dimensional Capillary, Reynolds, Weissenberg, Elasticity, and Dean numbers are described in ESI equations S1-S5. For square and rectangular channels, the mean hydraulic diameter, D_H, is used as the characteristic length term in the non-dimensionalized equations defined as $D_H = 4A/P = 2hw/(h+w)$.

Oil phase and tuning of κ

FC-40 (Sigma, USA) with dynamic viscosity, μ_o, of 4.1 cPs @ 25 ºC and density, ρ, of 1.85 kg/m^3 was selected as the continuous oil phase because of its low viscosity. This low viscosity oil was desired because it would require a smaller change in a droplets absolute viscosity to induce a large change in the viscosity ratio, $\kappa = \mu_i/\mu_o$. The value of 4.1 cPs is much closer to that of pure water with a dynamic viscosity of 1 cPs at 20 ºC. The viscosity of the aqueous phase was tuned through the addition of two Newtonian viscous enhancing additives, glycerol (EMD Chemicals, USA) and Ficoll® 400 with M_w 400,000 (Sigma, USA); and two non-Newtonian additives, poly-ethylene oxide or Polyox® WSA N-10 with Mw 100,000 (Amerchol Corp., USA), and anhydrous trimethyl-glycine also known as TMG or betaine (Purebulk, Oregon USA). Fluid viscosities of the aqueous and oil phase solutions were determined from measurements performed using a Physica MCR301 Rheometer using a 25mm CP 25-2/S

sandblasted measuring cone with a 2° angle (Anton Parr, USA) at shear rates ranging from 0.1 to 1,000 s^{-1}. Shear stress vs. shear rate information was characterized using the Rheoplus rheometer software to estimate the average fluid viscosities of the solutions.

Interfacial tension

The interfacial tension of the two fluids were modified through the use of a fluorosurfactant called Krytox 157 FSL (Dupont Chemicals, USA), and 1H,1H,2H,2H-perfluoro-1-Octanol (Sigma Aldrich, USA). Krytox is a long chain perfluoropolyether terminated with a carboxylic acid at one end that can be added in high concentrations to reduce the interfacial tension between water and oil. It also has a much higher viscosity than FC-40 and raises the viscosity of the oil phase with increasing concentrations. During the experiments, effective droplet stabilization and final viscosities were achieved using 7% Krytox and 0.05% perfluoro-octanol dissolved in FC-40. The octanol surfactant has a much lower viscosity and is effective at lowering interfacial tension but is also a hazardous material so special care was used when handling and concentrations were limited to extremely low values. More stable and biocompatible fluorosurfactants have been developed[44,45] but were not readily available for experimentation.

Results and Discussion

Fluid viscosity characteristics

Viscosity vs. shear rate measurements were performed for a range of Newtonian additive concentrations including Mw $4x10^5$ Ficoll, and glycerol, and Non-Newtonian additives including Mw $1x10^5$ PEO, and trimethyl glycine, whose η_∞ vs. concentration profiles are plotted in ESI Figure S4. Due to the low polymer/additive concentrations used in these experiments, the ability to characterize the viscoelastic behavior of the solutions was beyond the sensitivity of the rheometer. However, prior literature characterizing PEO solutions with various concentrations and molecular weights have been performed and are referenced to help describe their viscoelastic properties[46–48]. Work by Ebagninin et al. (2009) indicates that viscoelasticity of PEO solutions are highly dependent on both concentration and Mw of the PEO polymer, and could be well described using the Cross-Model to estimate a relaxation rate λ[49]. In their work however, they found that the same low molecular weight PEO solutions used in these experiments, Mw=$1x10^5$ (g mol^{-1}), exhibited near complete Newtonian properties, even up to 20% concentration (cone and plate geometry 60 mm diameter and 0.017 rad angle). Their rheometer measurements were also unable to demonstrate any detectable level of viscoelasticity of similar PEO solutions within the shear-stress sensitivity of their experimental setup.

Based on their experimental results for higher Mw $4x10^5$ PEO, relaxation rates λ for 1% wt./wt. concentrations did not exceed 0.0012 s, with the lowest value of λ = 0.0005 s for a 0.25% concentration. It is expected then, that a 1-2% solution of Mw $1x10^5$ PEO should have a λ-value lower than this number. Similar for TMG solutions, even at 33% wt./wt. concentrations, no viscoelasticity was observed within the shear stress sensitivity of the rheometer system. Based on this weak viscoelasticity, it is difficult to estimate the non-dimensional Elasticity and Weissenberg numbers of the experimental conditions, but it can be assumed that they are $\ll 1$. Despite the dilute concentrations of PEO and TMG, noticeable changes in the experimental migration direction of the droplets were still observed.

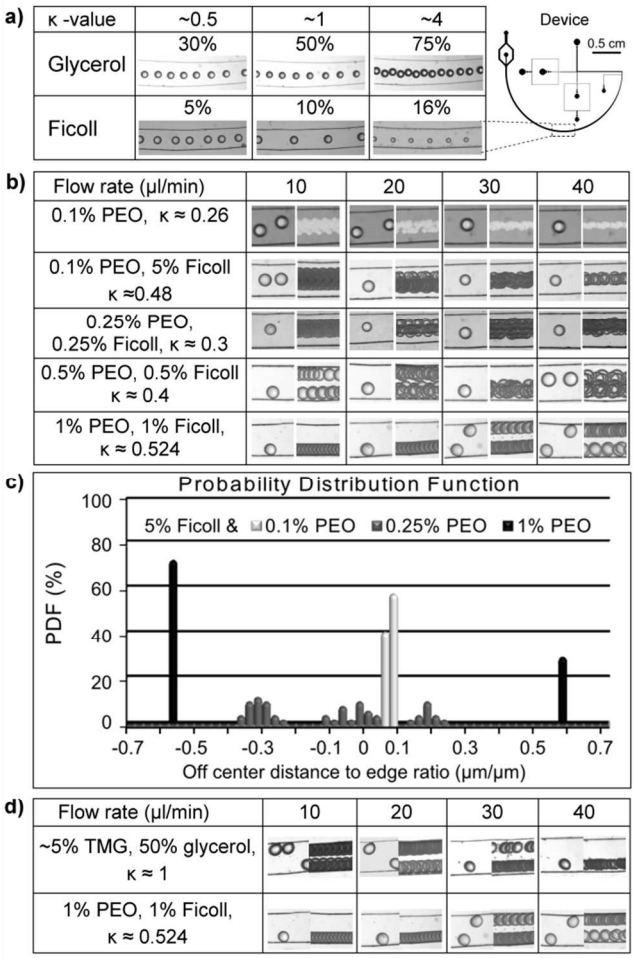

Fig. 3 Equilibrium positions of droplets containing various fluids. **a)** Newtonian fluids migrate to centerline of channel for varying κ -values from 0.2 to 4, flow rate 20 µL/min. Inset shows channel design, see ESI Figure S2 for more detail. **b)** Normal and composite overlay images of droplet equilibrium position as a function of polymer concentration and flow rate. **c)** Probability distribution function of droplet equilibrium position seen in b) as a function of Newtonian and viscoelastic polymer concentration at a constant flow rate, all droplets contain 5% Ficoll. **d)** Strong viscoelastic migration toward the edge is observed over a large range of flow rates when TMG and PEO concentrations are high and their viscosity ratios yield a negative α-value. Note on cchannel dimensions: spiral channels with radius of curvature R ≈ 1 cm, gradually widening at a rate of ~50 µm/cm. 180 µm wide x 100-110 µm height at point of measurement L ≈ 1.7 cm downstream. Flow rate: 10-40 µl/min; a/d ~ 0.4-0.5; Ca=~0.008 and Re=~0.8 at 20 µL/min flow rates.

Newtonian fluid equilibrium position at channel centerline

As seen in Figure 3-a), Newtonian fluids migrate toward the centerline of the channel, despite having κ-values that should produce a negative α value if the solutions were viscoelastic. It was found that for droplets ranging from 30-100 µm, effective droplet sorting occurred early on in the channel and typically did not require channel lengths longer than 1-2 cm to reach near equilibrium positions. Smaller droplets would require longer channel lengths, 7 cm or more, before observing their final equilibrium positions within the channel. It is notable that in this

central region of the channel, droplets are traveling at a higher velocity and settle into well-established linear streams of droplets that collide infrequently with other droplets. Despite the large range of κ-values, droplet sizes and flow rates, Newtonian droplets all behave similarly and migrate toward the channel centerline even though the migration rate may change.

Viscoelastic fluid equilibrium vs. Shear rate

In the experimental results, varying degrees of droplet migration behavior were observed depending on shear gradient profiles, fluid viscoelasticity, and fluid flow rate, as demonstrated in Figures 3-b), 3-c) & ESI Figures S5 and S6. One concept that is uncertain from Chan and Leal's theoretical work with second-order fluids is how well it relates to viscoelastic fluids and how strong of a viscoelastic effect is required to exhibit the migration characteristics desired. Similarly, equations 1 & 2 do not account for the shear rate-dependence of fluid viscosity. Three important misunderstood parameters with regard to fluid viscoelasticity and shear gradient profile were found to effect droplet migration. (1) What is the nature of the viscoelasticity and the overall range of shear-rate dependent viscosity? (2) What is the localized shear gradient profile to which the droplet is exposed? (3) What is the global shear rate the droplet experiences? Unfortunately, current literature is sparse with regard to viscoelastic droplet migration relating to these conditions, with only minimal information available for second-order fluids or shear-thinning fluids.

As observed in Figure 3-b) & 3-c), increasing the total PEO concentration results in a transition in the migration of droplets from the center of the channel towards the edge, which follows the predicted behavior of an increasingly viscoelastic fluid. With low PEO concentration of 0.1%, a slight off-center equilibrium position develops in the droplets. Increasing PEO concentrations to 1%, a stronger viscoelasticity drives the droplets all the way to the edge with great reproducibility. One interesting observation during experimentation is that with intermediate viscoelasticity, increasing the total flow rate shifts the equilibrium position away from the edges and closer to the centerline.

With the addition of 5% Ficoll to the 0.1% PEO concentration, cross-lateral migration is only slightly changed despite the higher κ-value, indicating the fluid is not sufficiently viscoelastic. This would also indicate that the observed flow rate dependent behavior has a high level of dependence on the overall shear rates to which the aqueous droplet phase is exposed and the characteristic relaxation rates of the solutions. As demonstrated in the work by Ebagninin et al. (2009), the infinite and zero viscosities and the characteristic relaxation times of PEO solutions were found to increase with increasing PEO concentration. This indicates that low PEO concentrations may be sufficient to cause some viscoelastic effect and drive the droplets off center, but their relaxation rates are fast and weak, making the effect insufficient to drive them into higher shear rates near the channel wall. Figure 3-d) shows experimental conditions that favor strong viscoelastic droplet migration when using sufficient TMG or PEO concentrations and κ-values that provide a negative α value.

Based on the results illustrated in Figures 3-b), 3-c) and ESI figure S5, it is proposed that a greater majority of the droplet is exposed to shear gradients above the characteristic relaxation rate as the overall flow and shear rate is increased. It would follow

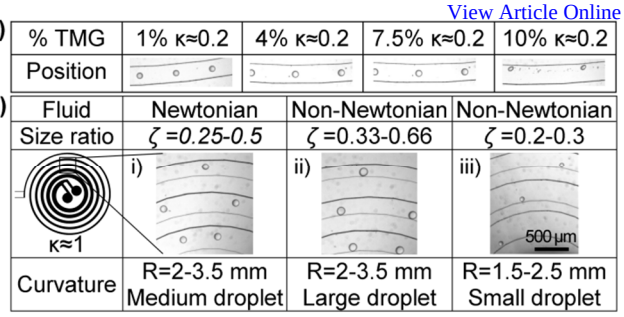

Fig. 4 a) Equilibrium position of droplets containing increasing concentrations of TMG but with near constant κ-value of ~1. Despite undetectable changes in viscosity ratio κ, the droplet position shifts from centerline to the edge. **b)** Curved, gradually widening channels with radius of curvature R=1.5-3.5 mm, channel height is 84 μm, width varies from i) 170- 260 μm ii) 170- 260 μm , and iii) 220- 300 μm from top to bottom. Flow rate is 13 μL/min with i) 50% glycerol, ii) and iii) have 50% glycerol & 1% PEO. ζ = a/d droplet diameter vs. channel width. Continuous phase is light mineral oil. See supplemental Video S1 and S2 that illustrate conditions i) and ii) respectively.

that if the localized shear rate is low, the viscosity of the droplet phase will be dominated by the viscoelasticity of the fluid, and the droplet will experience cross-lateral migration toward the wall. If the localized shear rate is high relative to the relaxation rate, the viscosity of the droplet will be dominated by the Newtonian properties of the fluid at infinite shear viscosity. This would then cause the droplet to experience cross-lateral migration toward the channel centerline as if mostly Newtonian, but still remain slightly off center. In microfluidic channels with flow rates as low as 10 μL/min, global shear rates may range from near zero at the centerline, to $\dot{\gamma} > 1\text{x}10^4$ at the edge, assuming a no slip boundary condition. Depending on the droplet position and its size relative to the channel width, the overall shear gradient to which the droplet is exposed will vary. This would explain why droplets would not only migrate to the wall or the channel, but may also exhibit equilibrium positions between those two points, See ESI section II for more discussion.

Viscoelastic migration outside of the predicted κ -value

TMG was selected as a low viscosity viscoelastic additive. Experimental results shown in Figure 4-a) illustrate that, contrary to what was expected for the range of κ-values predicted by Chan and Leal, the addition of more TMG to the droplet phase resulted in migration toward the channel edge despite having measured κ -values of 0.2. This characteristic behavior seems to correspond with that of Sullivan et al. (2008) where bubbles with high viscoelasticity and low interfacial tension experienced transverse migration toward the channel wall despite having an expected κ-value $\ll 1$. A noteworthy fact is that higher concentrations of TMG also reduce the interfacial tension between the fluids thereby reducing the Laplace pressure inside the droplet and increasing droplet deformability as evident from equation 1. These results suggest that the model presented by Chan and Leal described in equations 1 & 2 does not adequately describe droplet migration properties for all fluid conditions.

Droplet size and channel curvature dependent migration

As described in the theoretical section and shown in equation 1, a larger droplet diameter will experience greater droplet migration rates. As a result, the overall droplet position vs. channel length

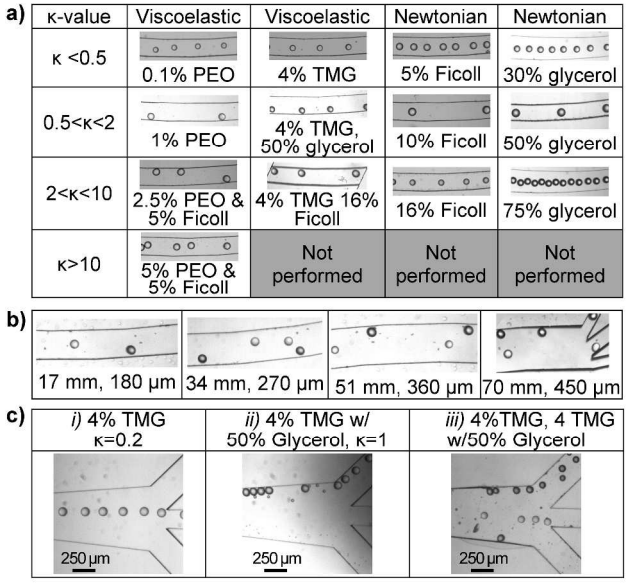

Fig. 5 a) Summary of viscoelastic droplet sorting after 17 mm downstream propagation for different fluid viscosities and viscoelastic conditions. Channel dimension: 180 um wide x 100 um height; flow rate = 20-30 μl/min; ζ=0.4-0.5; Ca=0.008 and Re=0.8. **b)** Efficient separation of viscoelastic droplets with two different κ -values. Light colored circles contain 4% TMG, and dark circle droplets contain 4% TMG w/ 50% glycerol. Equilibrium position is established early on, before 17 mm, and continues until separation at the outlet positioned 70 mm downstream. Q = 20 μL/min, R=1 cm, h=84 μm, **c)** Sorting of viscoelastic droplets in curved channels with different κ-values corresponding to a 1 cPs & 5 cPs droplet viscosity. i) viscoelastic droplets with κ=0.2 exit center channel, ii) viscoelastic droplet with κ=1 exit top and bottom channel, iii) separation of viscoelastic droplets with κ=0.2, and κ=1 into separate outlet channels. Channel width gradually increases from 60 μm to 250 μm along a 2 cm long channel then quickly expands to 500 μm at the three-way outlet. Conditions: R=1 cm, Q=30 μL/min, h=107 μm. Droplet generation rates were varied from 30-250 drops/sec in 15:1 to 1:15 droplet ratios and enrichment factors obtained varied from 5 to >100.

is dependent on droplet size. Similarly, a large droplet size relative to a given channel dimensions will have a more significant contribution to the localized flow profile resulting in local variations in shear gradients, see ESI section II for more discussion. For this reason, droplet sizes were kept to no larger than the smallest channel dimension during experimentation to reduce spurious effects resulting from excessive droplet feedback, in most cases 100 μm, but also kept larger than 30 μm to yield faster migration rates. Droplet migration in curved channels with varying radius of curvature, cross-sectional diameter, and droplet/channel width ratio, ζ, is shown in Figure 4-b) and ESI video S1 and S2; channel dimensions are further illustrated in ESI figure S2-d). These results demonstrate that predictable droplet migration is achieved in rectangular channels with heights of 84-110 μm, droplet sizes of 30-100 μm, channel w/h aspect ratios of 0.5-5, droplet diameter to channel width aspect ratios of ζ = 0.17-0.66, channel curvature from straight to 1.5 mm curvature, and flow rates ranging from 10-40 μl/min.

Favorable operating parameters for droplet sorting

An effective range of droplet sorting parameters has been determined as summarized in Figure 5-a) showing Viscoelastic and Newtonian droplet equilibrium positions for different κ-values ranging from 0.2-20. Similar to the theory predicted in equations 1 & 2, droplet migration tends toward the edge when moderately viscoelastic and $0.5 < \kappa < 10$, otherwise migration tends toward the centerline for most other conditions. However, from the results shown in Figure 5-a), there are exceptions to this behavior and they should not be overlooked. Future work might include exploration into whether traditional pinched flow based hydrodynamic sorting could be applied to droplet viscosity polydispersity much like it has been to droplet size polydispersity[4,9]. This would enable the enrichment of droplets with a broad range of viscosities that do not follow a bi-modal distribution.

Droplet Enrichment

Effective droplet enrichment was achieved with a droplet population consisting of 4% TMG (bright droplet), and 4% TMG w/ 50% glycerol (dark droplet) sorted at the outlet as shown in Figure 5-b) & 5-c). These formulations behave similar to Ficoll and PEO as shown in figure 5-a). Videos illustrating droplet generation, injection into the sorting channel, and equilibrium positions near the outlet are shown in ESI videos S3 and S4. Sorting rates of >200 drops/sec were achieved based on 75 μm droplets with average droplet generation rates of 250 drops/s for positive migration droplets and 185 drops/s for negative migration droplets. Sorting enrichment factors >100 were achieved using 20-40 μL/min oil flow rates in a 0.5 cm long straight channel as shown in ESI Figure S2-c). Droplet enrichment factors were calculated for 1,000 drops generated at a ratio of ~4:3 positive/negative migration droplets that were measured to exit the channels at a ratio of ~1/166 in the positive migration outlet and ~180/1 in the negative migration outlets, resulting in enrichment factors of ~125 and ~240 respectively. See ESI videos S5 and S6 for examples of droplet sorting at the outlet. Although the sorting design allows for droplets migrating towards the center to pass around droplets against the edge, droplet-droplet interactions among viscoelastic droplets at the edge resulted in poorer sorting efficiencies. Future efforts to optimize sorting rates and reduce droplet-droplet interactions would help to improve these sorting efficiencies.

Other future work might include enrichment of specific droplet viscosities into multiple outlets using pinched flow like hydrodynamic sorting based on varying alpha values resulting in similarly varying droplet migration rates. This could prove useful for, e.g., separating cells that secrete viscosity changing proteins or molecules at different rates or concentrations. Actively tuned droplet sorting parameters might also be implemented such as the use of optically induced crosslinking or temperature regulation, which could influence viscosity, interfacial tension, or droplet deformability. Photo-activated crosslinking agents might be useful to induce viscosity changes within droplets of interest at various stages of fluid handling. Similarly, by controlling the temperature at which sorting is performed; viscosity ratios could be further varied to achieve even more sensitive discrimination factors between two viscous droplet populations.

Conclusions

These experimental results demonstrate a moderate size-independent droplet sorting behavior that can separate monodisperse droplets of the same viscosity ratio but different

viscoelasticity, or two similarly viscoelastic droplets but with different viscosity ratios. This is demonstrated for κ values ranging from 0.2 to 5, with effective sorting capable at viscosity discriminations as low as 3 cPs if using low viscosity oils such as fluorocarbon-based fluids. Effective droplet migration toward the channel edge was achieved by controlling the rectangular channel geometry, flow profile, viscoelasticity, and w/o fluid viscosity ratios. Droplets could be distinguished with greater than 100 fold enrichment factors and discrimination in viscosity changes could be detected from 1 to 4 cPs corresponding to a change in κ from 0.2-0.8. Droplet flow rate and inter-droplet spacing is important for improved droplet sorting efficiency, especially in the case of high concentrations of droplets that migrate toward the channels edge. Reducing interfacial tension, as seen with TMG, tends to increase droplet deformability and results in droplet migration even at κ-values as low as 0.2. Additives that change the viscosity of the fluid can be useful to tune the sorting efficiency of the aqueous droplets.

The passive and intrinsic nature of this sorting scheme should prove useful for enrichment or detection of chemical, biological, or biochemical samples in which a degradation, polymerization, or protein binding reaction occurs, resulting in a heterogeneous change in droplet viscosities. It also provides a look into viscoelastic behavior and instability problems that may be associated with other droplet microfluidic platforms that will expand to utilize a greater variety of biological samples.

Future research efforts to implement this sorting technique with biologically relevant assays could include alginate cross-linking or degradation[50], PCR amplification[51–53], protein cross-linking[54], blood clotting[55], and others[7]. Similarly, other effects that might influence sorting behavior, such as temperature control, would be interesting phenomena to explore. Information gathered from this work could be further expanded to implement sorting of a polydisperse droplet viscosity population, or combined with other sorting techniques for greater sorting abilities. These techniques may also prove useful for other applications such as to determine the viscoelastic nature of weakly viscoelastic fluids since it appears to be sensitive to additives that yield virtually undetectable viscoelastic properties using commonly available commercial instruments.

Acknowledgements

The authors thank Dr. Jeffrey S. Fisher and Dr. Arezoo M. Ardekani for technical contributions to the work. This work was performed under the auspices of the U.S. Department of Energy by Lawrence Livermore National Laboratory under Contract Contract DE-AC52-07NA27344. This work was also supported in part by the Defense Advanced Research Projects Agency (DARPA) N/MEMS S&T Fundamentals Program under grant no. N66001-1-4003 issued by the Space and Naval Warfare Systems Center Pacific (SPAWAR) to the Micro/nano Fluidics Fundamentals Focus (MF3) Center.

Notes and References

[a] *Biomedical Engineering, 3120 Natural Sciences II, University of California-Irvine, 92697, USA. Fax: 949 824-1727; Tel: 1-949-824-9691; E-mail: aplee@uci.edu, ahatch@uci.edu*

[b] *Center for Micro- and Nanotechnologies; Lawrence Livermore National Laboratory, Livermore, CA 94550, USA*

[c] *Mechanical & Aerospace Engineering, University of California, Irvine*

† Electronic Supplementary Information (ESI) available: ESI contains information on equations, theory, operational parameters and supplementary figures to describe microfluidic designs and shear sorting results. See DOI: 10.1039/b000000x/

1. X. Niu, M. Zhang, S. Peng, W. Wen, and P. Sheng, *Biomicrofluidics*, 2007, **1**, 44101.
2. K. Ahn, C. Kerbage, T. P. Hunt, R. M. Westervelt, D. R. Link, and D. A. Weitz, *Applied Physics Letters*, 2006, **88**, 024104.
3. Y.-C. Tan, Y. L. Ho, and A. P. Lee, *Microfluidics and Nanofluidics*, 2008, **4**, 343–348.
4. M. Chabert and J.-L. Viovy, *Proc. Natl. Acad. Sci. U. S. A.*, 2008, **105**, 3191–3196.
5. Y. C. Tan, J. S. Fisher, A. I. Lee, V. Cristini, and A. P. Lee, *Lab Chip*, 2004, **4**, 292–298.
6. J.-C. Baret, V. Taly, M. Ryckelynck, C. A. Merten, and A. D. Griffiths, *Med Sci (Paris)*, 2009, **25**, 627–632.
7. S. Y. Teh, R. Lin, L. H. Hung, and A. P. Lee, *Lab Chip*, 2008, **8**, 198–220.
8. J.-C. Baret, O. J. Miller, V. Taly, M. Ryckelynck, A. El-Harrak, L. Frenz, C. Rick, M. L. Samuels, J. B. Hutchison, J. J. Agresti, D. R. Link, D. A. Weitz, and A. D. Griffiths, *Lab Chip*, 2009, **9**, 1850–1858.
9. C.-H. Yang, Y.-S. Lin, K.-S. Huang, Y.-C. Huang, E.-C. Wang, J.-Y. Jhong, and C.-Y. Kuo, *Lab Chip*, 2009, **9**, 145–150.
10. Y. C. Tan and A. P. Lee, *Lab Chip*, 2005, **5**, 1178–1183.
11. Y.-C. Tan, V. Cristini, and A. P. Lee, *Sensors and Actuators B: Chemical*, 2006, **114**, 350–356.
12. I. Kobayashi, K. Uemura, and M. Nakajima, *Langmuir*, 2006, **22**, 10893–10897.
13. A. Karnis and S. G. Mason, *Trans. Soc. Rheol.*, 1966, **10**, 571–592.
14. F. Gauthier, H. L. Goldsmith, and S. G. Mason, *Trans. Soc. Rheol.*, 1971, **15**, 297–330.
15. B. P. Ho and L. G. Leal, *Journal of Fluid Mechanics*, 1976, **76**, 783–799.
16. P. C.-H. Chan and L. G. Leal, *Journal of Fluid Mechanics*, 1979, **92**, 131–170.
17. P. C.-H. Chan and L. G. Leal, *International Journal of Multiphase Flow*, 1981, **7**, 83–99.
18. L. G. Leal, *Journal of Non-Newtonian Fluid Mechanics*, 1979, **5**, 33–78.
19. S. D. Hudson, *Phys. Fluids*, 2003, **15**, 1106.
20. J.-P. Matas, J. F. Morris, and éLisabeth Guazzelli, *Journal of Fluid Mechanics*, 2004, **515**, 171–195.
21. W. S. J. Uijttewaal, E.-J. Nijhof, and R. M. Heethaar, *Phys. Fluids A*, 1993, **5**, 819–825.
22. V. Cristini and Y. C. Tan, *Lab Chip*, 2004, **4**, 257–264.
23. K. Feigl, D. Megias-Alguacil, P. Fischer, and E. J. Windhab, *Chemical Engineering Science*, 2007, **62**, 3242–3258.
24. W. Li, G. H. Ko, and D. Gersappe, *Physical Review E - Statistical, Nonlinear, and Soft Matter Physics*, 2005, **72**, 066305.
25. M. Shapira and S. Haber, *International Journal of Multiphase Flow*, 1990, **16**, 305–321.
26. A. M. Leshansky, A. Bransky, N. Korin, and U. Dinnar, *Phys. Rev. Lett.*, 2007, **98**, 234501.
27. E. S. Asmolov, *Journal of Fluid Mechanics*, 1999, **381**, 63–87.
28. J. Oakey, R. W. Applegate, E. Arellano, D. D. Carlo, S. W. Graves, and M. Toner, *Analytical Chemistry*, 2010, **82**, 3862–3867.
29. D. R. Gossett and D. D. Carlo, *Analytical Chemistry*, 2009, **81**, 8459–8465.
30. D. Di Carlo, *Lab Chip*, 2009, **9**, 3038–3046.
31. D. Di Carlo, D. Irimia, R. G. Tompkins, and M. Toner, *Proc. Natl. Acad. Sci. U. S. A.*, 2007, **104**, 18892 –18897.
32. S. Yang, J. Y. Kim, S. J. Lee, S. S. Lee, and J. M. Kim, *Lab Chip*, 2011, **11**, 266–273.
33. Y.-S. Choi, K.-W. Seo, and S.-J. Lee, *Lab Chip*, 2011, **11**, 460–465.
34. C. Coulliette and C. Pozrikidis, *Journal of Fluid Mechanics*, 1998, **358**, 1–28 M3 – null.

35. S. C. Hur, H. T. K. Tse, and D. Di Carlo, *Lab Chip*, 2010, **10**, 274–280.
36. S. C. Hur, N. K. Henderson-MacLennan, E. R. B. McCabe, and D. Di Carlo, *Lab Chip*, 2011, **11**, 912–920.
37. S. K. Doddi and P. Bagchi, *International Journal of Multiphase Flow*, 2008, **34**, 966–986.
38. J. R. Smart and J. Leighton, *Phys. Fluids A*, 1991, **3**, 21–28.
39. M. Shapira and S. Haber, *International Journal of Multiphase Flow*, 1988, **14**, 483–506.
40. A. J. Griggs, A. Z. Zinchenko, and R. H. Davis, *International Journal of Multiphase Flow*, 2007, **33**, 182–206.
41. M. T. Sullivan, K. Moore, and H. A. Stone, *Phys. Rev. Lett.*, 2008, **101**, 244503.
42. G. M. Whitesides, E. Ostuni, S. Takayama, X. Jiang, and D. E. Ingber, *Annual Review of Biomedical Engineering*, 2001, **3**, 335–373.
43. Y. Xia and G. M. Whitesides, *Annual Review of Materials Science*, 1998, **28**, 153–184.
44. D. J. Holt, R. J. Payne, W. Y. Chow, and C. Abell, *Journal of Colloid and Interface Science*, 2010, **350**, 205–211.
45. C. Holtze, A. C. Rowat, J. J. Agresti, J. B. Hutchison, F. E. Angile, C. H. J. Schmitz, S. Koster, H. Duan, K. J. Humphry, R. A. Scanga, J. S. Johnson, D. Pisignano, and D. A. Weitz, *Lab Chip*, 2008, **8**, 1632–1639.
46. K. W. Ebagninin, A. Benchabane, and K. Bekkour, *Journal of Colloid and Interface Science*, 2009, **336**, 360–367.
47. D. M. Yu, G. L. Amidon, N. D. Weiner, and A. H. Goldberg, *J. Pharm. Sci.*, 1994, **83**, 1443–1449.
48. O. Arnolds, H. Buggisch, D. Sachsenheimer, and N. Willenbacher, *Rheol Acta*, 2010, **49**, 1207–1217.
49. M. Cross, *Journal of Colloid Science*, 1965, **20**, 417–437.
50. H. Zhang, E. Tumarkin, R. Peerani, Z. Nie, R. M. A. Sullan, G. C. Walker, and E. Kumacheva, *J. Am. Chem. Soc.*, 2006, **128**, 12205–12210.
51. A. Goodman, Y. Tseng, and D. Wirtz, *Journal of Molecular Biology*, 2002, **323**, 199–215.
52. X.-D. Yang and R. V. N. Melnik, *Computational Biology and Chemistry*, 2007, **31**, 110–114.
53. D. M. Curtin, D. T. Newport, and M. R. Davies, *Experimental Thermal and Fluid Science*, 2006, **30**, 843–852.
54. G. Lemercier, S. Gendreizig, M. Kindermann, and K. Johnsson, *Angewandte Chemie International Edition*, 2007, **46**, 4281–4284.
55. H. Song, H.-W. Li, M. S. Munson, T. G. Van Ha, and R. F. Ismagilov, *Anal. Chem.*, 2006, **78**, 4839–4849.